GPR surveys for the prevention of karst risk in underground gypsum quarries

GPR surveys for the prevention of karst risk in underground gypsum quarries.

Caselle Chiara[1] – chiara.caselle@unito.it

Bonetto Sabrina[1] – sabrina.bonetto@unito.it

Comina Cesare[1] – cesare.comina@unito.it

Stocco Stefano[2] – stocco@gamutgeophysics.com

1 – Department of Earth Sciences - DST, Università degli Studi di Torino, via Valperga Caluso 35, Torino, 10125, Italy

2 - GAMUT S.r.l., via Lamarmora 16, Torino, 10128, Italy

Corresponding Author: Caselle Chiara, chiara.caselle@unito.it – Department of Earth Sciences - DST, Università degli Studi di Torino, via Valperga Caluso 35, Torino, 10125, Italy

Abstract

The investigation and prediction of geological anomalies in underground quarries is fundamental to ensure safety, efficiency and economic convenience of the exploitation. For these aims, non-destructive geophysical surveys may be an effective alternative approach to classical destructive prospecting techniques (i.e. horizontal drilling), with great advantages particularly in complex geological frameworks and in areas subjected to specific geo-hazards. Ground Penetrating Radar (GPR), for its high resolution, is a suitable technique for underground excavations, particularly for the identification of water bodies, fissures and fractured rocks. The present study is focused on the application of GPR for the prediction of karst structures in underground gypsum quarries. Karst phenomenon is a main risk factor for gypsum orebodies, where large cavities may be intersected by the excavation. The possible filling with clay or pressurized water of these cavities exponentially increases the dangerousness of the phenomenon, due to swelling problems and violent water inrushes. The aim of the present study is to propose, through modelling and field surveys, a description of GPR outputs for principal elements of karst hazard in gypsum bodies, with particular attention to the discrimination of fillings (air, water or clay).

Keywords: GPR, Gypsum, Karst, Underground exploitation

1. Introduction

In underground mining activities several geological problems can interfere with excavation safety, environmental sustainability and the general efficiency in the exploitation of resources.

The mining site safety can be endangerment, *in primis*, by mechanical and structural features of the rock mass. In this framework, for instance, structural weaknesses may cause the split-up of instable blocks, with generation of collapses, or may decrease the stability of the underground drifts, by damaging support elements such as pillars or walls. These weaknesses usually manifest with ongoing fracturing at the excavation front or within the rock mass. In gypsum orebodies, other problems, due to the presence of karst phenomena and pressurized water in fractures or caves, can arise. Violent water inrushes connected with karst phenomenon may cause serious consequences in both environmental and safety fields. Several research groups dealt with tunnel instability induced by large-scale karst phenomenon, trying to determinate the minimum safety thickness of tunnel rock walls for resisting water inrushes (e.g. Jiang et al., 2017; Xu et al., 2018; Wu et al., 2019). The possibility to forecast the presence of karst voids and to understand the nature of filling materials (air, water or clay) has therefore a relevant interest. The use of indirect geophysical methods offers some advantages in terms of repeatability and rapidity, representing an alternative method to classical destructive prospecting techniques (i.e. horizontal drilling).

Among geophysical methods, Ground Penetrating Radar (GPR) is an electromagnetic technique primarily designed for location of objects or interfaces buried beneath the earth's surface or located within a visually opaque structure (Daniels, 2004). The application of this technique is based on the propagation and reflection of a high frequency (10 MHz – 2.5 GHz) electromagnetic signal. GPR has been used since mid 90s for applications in civil engineering, but it is with the technological advancements and tremendous improvements of digital computation power in the last decades that GPR applications had a blossoming. Several application fields can be remembered including geotechnical applications (Wai-Lok Lai et al., 2018).

An important application field of GPR is the localization of water content zones (Afshar et al., 2015; Bowling et al., 2005; Mahmoudzadeh et al., 2012) and of morphologies connected to karst phenomena, such as cavities and buried sinkholes (Afshar et al., 2015; Gómez-Ortiz and Martín-Crespo, 2012; Pueyo-Anchuela et al., 2015; Sevil et al., 2017). Pueyo-Anchuela et al. 2009 codified the GPR key-features of some karst-connected morphologies (i.e. sediment-filled cavities, evidences of subsidence and paleo-collapses). They propose a "guide" to recognize these morphologies in GPR profiles acquired from the surface, describing the expected geometrical relations among electromagnetic reflectors (i.e. on-lap geometries, depressed reflectors, folded reflectors or laterally abrupt changes of electromagnetic properties).

GPR method has been proposed and used for the assessment of fracturing and mechanical damage in tunnel ahead prospecting, both in civil and mining frameworks, offering high resolution images about the material behind the excavation face. Compared to seismic methods used for the same purposes, GPR provides higher resolution data but lower penetration depth (Li et al., 2017). In particular, in mining environments, both during the mining design and the mining exploitation, the detailed knowledge of the rock mass produced by GPR can indeed be of primary utility. As an example, in this context, GPR has been already used to detect the presence of fractures (e.g. Kovin, 2011; Porsani et al., 2006) and to infer the presence of microcracks and to evaluate the rock mass quality (e.g. Dérobert and Abraham, 2000; Orlando, 2003). Kadioglu, 2008 suggested to apply this methodology to recognize layers with different geological features. Aldas et al., 2006 proposed a method to use GPR to obtain the subsurface images of rock discontinuities in order to improve the design of the blasting pattern.

The present study proposes the application of GPR to forecast karst morphologies and to discriminate their fillings in underground gypsum quarries. The low primary porosity of gypsum and the possibility to have fluid circulation connected with secondary permeability (due to fractures or discontinuities) frequently bring to the formation of karst phenomena in this material. GPR techniques were applied

to the identification of the principal risk factors connected with karst phenomenon in underground excavations and to the discrimination of filling materials (air, water or clay). Both modeled and experimental data acquired in two test sites are hereafter presented.

2. Test sites: geological framework

The test sites are two gypsum quarries located in the Monferrato area (Piedmont, NW Italy): Moncalvo quarry and Calliano quarry (Figure 1a). From a geological point of view, they are sited in the Tertiary Piedmont Basin (TPB), a Late Eocene - Miocene complex sedimentary basin (Clari et al., 1995; Piana and Polino, 1995). Gypsum beds are dated to Late Messinan age, when the so called "Messinian Salinity Crisis" occurred (Dela Pierre et al., 2011). The stratigraphic characteristics of the area see the gypsum unit sandwiched between marl and clayey sediments.

The quarries are exploited through underground excavations. The ore bodies consist of 4 gypsum layers, each about ten meters thick, divided by marl layers a few meters thick (Figure 1b). Stratigraphic discontinuities separating gypsum and marls layers dip to NW at low angle (10°-12°). Going from bottom to top, there are 3 macrocrystalline gypsum layers (massive selenite gypsum) and 1 microcrystalline gypsum layer (branching selenite gypsum). Nowadays, the exploitation is active in the first three layers from the top, while the macrocrystalline gypsum layer in the lower stratigraphic position is not in use. The quarries are therefore organized in three underground levels. The evaluation of mechanical properties for the stability assessment of the drifts is complicated by the gypsum anisotropy and heterogeneity in compositional and textural features (Caselle et al. 2018, Caselle et al. 2019a, Caselle et al. 2019b, Caselle et al. 2019c). The excavation works proceed using continuous mining machinery, represented by a road header, because of gypsum low mechanical resistance and abrasiveness and orebody regularity. The drifts do not intersect each other orthogonally as in a blasting exploitation, but take a "lozenge pattern", with a "rooms and rib pillars" exploitation planning (Figure 1c) (Bonetto et al., 2008). The resulting excavation faces are smooth, with a regular surface with average sizes of 6m x 6m, with rounded corners and a slight convexity. The advancement

of the road header machine produces residual "waves" in the lateral walls of the drifts (Figure 1d). Their amplitude (about 0.4 m) corresponds to the material exploited in each machine step.

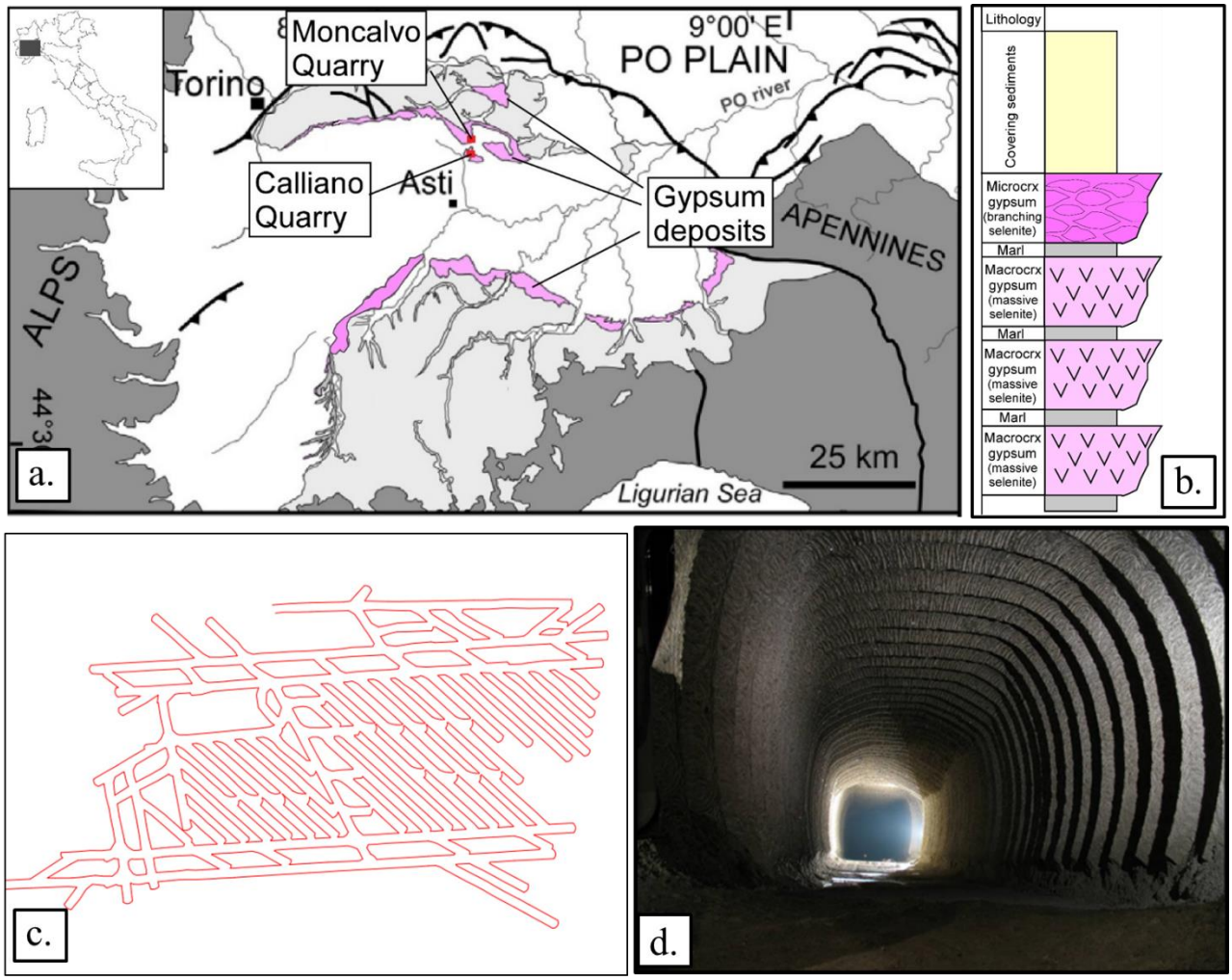

Figure 1 a. Areal distribution of gypsum deposits in northwester Italy and geographical localization of the test sites. b. Representative simplified stratigraphic column of the gypsum orebody. c. Lozenge drilling pattern for the excavation of gypsum with road header. d. Regular profile of the drilling drifts, with the "waves" produces by the machine advancement on the lateral walls.

Evidences of karst phenomena were recognized in the gypsum layers of both quarries. The scheme in Figure 2a illustrates the principal features of the karst circulation in the area. The karst system is controlled by the presence of pre-existing fracturing (with a mean sub-vertical orientation) copulated with the sub-horizontal stratigraphic discontinuities, separating gypsum and marls. The permeability contrast of these stratigraphic discontinuities favours the water circulation within the gypsum body and the consequent dissolution processes, leading to the development of the karst conduits and

cavities. The presence of peculiar features makes, however, the two situations quite different, as described by Vigna et al., 2017 (Fig. 2c-d).

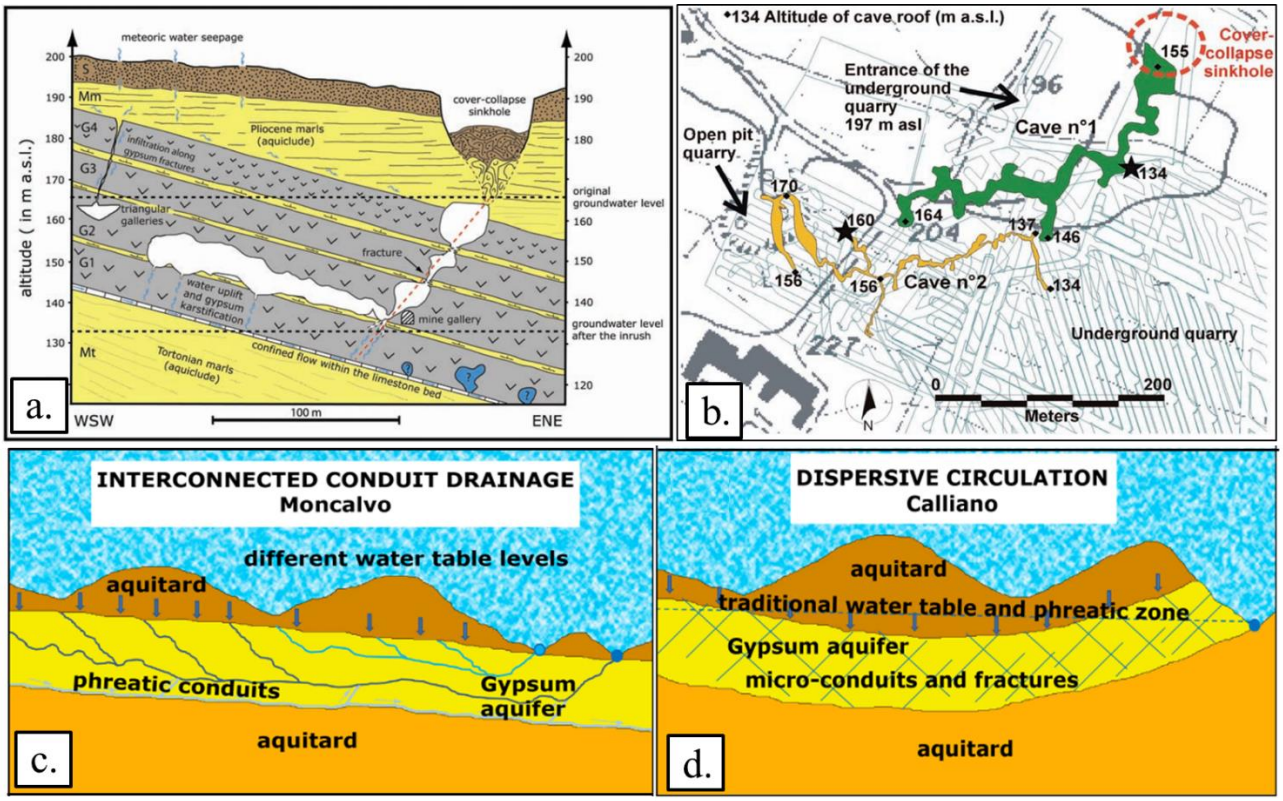

Figure 2 a. Scheme of the karst circuit characteristics in the gypsum body (Vigna et al. 2010; Bonetto et al., 2008) b. Moncalvo quarry map with the cartographical representation of the survived karst caves. The stars represent the points of intersection with the drifts (Vigna et al. 2010) c-d Conceptual models for karst circulation in gypsum (modified by Vigna et al., 2017):c. Interconnected conduit drainage karst system, recognized in Moncalvo quarry. d. Dispersive karst circulation system, recognized in Calliano quarry.

In the Moncalvo quarry (Fig. 2c) the gypsum sequence is relatively compact. Both surficial waters and rising fluids, following sets of fractures in the upper and lower rocks (aquitards), recharge the karst circuits, creating an underground water circulation within conduits and caves. In this quarry, the karst problem assumed a particular relevance since 15th February 2005, when the incidental intersection of a karst circuit during mining works caused an inrush of 60,000 m^3 of water mixed with mud causing the complete flooding of the lower quarry tunnels (Bonetto and Fornaro, 2005; Bonetto et al., 2008; Vigna et al., 2010). A big "camera" (a few hundred m^3) was identified in contact with the level 1 drift where the inrush happened. From this "camera", 850 meters of cave passages, characterized by typical phreatic morphologies, were observed (Fig. 2b). In this framework, the presence of karst conduits and karst caves is the principle cause of risk for the quarry activities. In

general, the dangerousness of these elements is determined by the filling. Particular attention is therefore paid to the presence of clay or pressurized water. The monitoring activity has to be directed mainly to the identification of karst caves shape and to the type of filling material.

A completely different hydrogeological situation can be found in Calliano quarry (Fig. 2d). Gypsum beds are characterized by a much more intense fracturing, with numerous small karst conduits and water-bearing fractures. Calliano is therefore a classical example of "dispersive karst circulation system", an extensively fractured and karstified aquifer with very good interconnection among fractures and karst conduits. In this case, the monitoring activity has to be directed mainly to the identification of small karst conduits and fractures, typically orientated vertically through the gypsum beds, with particular attention to the possibility of a filling material (clay) or to the presence of pressurized water.

3 Methodologies

Depending on the hydrogeological conditions and karst frameworks of gypsum orebodies, GPR modelling and field surveys were directed to evaluate GPR potentialities in the identification of the following elements:

- Karst conduits: despite their little diameters, they guarantee the alimentation of the karst circuit and the connection among the different parts of the network. They are potentially bearing large quantities of pressurized water;
- Karst cavities, with variable sizes from one to several cubic meters: their potential filling with clay or water constitutes the principal source of danger for underground excavations;
- Open fractures: they are preferential ways for water circulation and represent structural weaknesses for the rock-mass stability.

First, appropriate numerical models simulating the presence of all the above anomalies were produced. Three different anomaly fillings (air, water, clay) were simulated to evaluate their influence

on the resulting radargrams and their possible identification. To confirm the evidences of numerical models and to better evaluate the potentiality of GPR in the real quarry environment, field data were acquired in different locations within the quarries where known anomalies were recognized. Simulated and field radargrams were finally compared to allow for a combined evaluation of the GPR potentiality in this environment.

3.1 Modelling

Numerical modeling of the three types of identified anomalies in the gypsum rock-mass were developed and used to simulate the correspondent radar outputs. The code GprMax2D, based on a finite-difference time-domain numerical method, was used for numerical simulations.

Numerical modelling was developed along 2d sections (oriented as shown in Figure 3a). The gypsum orebody was simulated with appropriate electromagnetic features reflecting the average rock mass properties. The possible anomalies were simulated adding to the rock-mass model geometrical entities with the electromagnetic features of the desired filling (water, air or clay). Electromagnetic properties of both the gypsum orebody and the investigated anomalies are reported in Table 1. These parameters have been selected both on the analysis of experimental data and on the study of literature properties for the investigated materials. The cell sizes in the models (Δx and Δy) were chosen in order to minimize numerical dispersion, following

$\Delta x = \Delta y \leq \lambda/10$ and

$\Delta x = \Delta y < s/10$

where λ is the wavelength of the signal and s is the size of the smallest modelled object. Considering a central frequency of radar antenna of 200 MHz and the mean relative electrical permittivity of gypsum (from Table 1), the expected wavelength is 0.45 m. The smallest modelled object (karst conduit) has a diameter of 0.2 m. Therefore, cell sizes lower than 0.02 m allows for the respect both the thresholds.

Table 1 Relative electrical permittivity and electrical conductivity for the principal material involved in karst systems in gypsum beds.

	Relative electrical permittivity [ε_r]	Electrical Conductivity [σ/m]
"Macrocrystalline" Gypsum	11	0.67×10^{-2}
"Microcrystalline" Gypsum	11	1.25×10^{-2}
Air	1	0
Water	80	0.25
Clay	8	2.5×10^{-2}

Over these constructed models, the GPR acquisition was simulated by passing the appropriate radar antenna (modelled as a line source) from the left to the right. Signal was simulated as a ricker wave, with central frequency of 200 MHz. Adsorbing Boundaries were included in the models at a certain distance from the investigated area (usually at least 15 cells) to avoid artificial reflections at model borders. Synthetic radargrams were therefore computed as the z-component of the electromagnetic field (perpendicular to the quarry face).

Synthetic radargrams were produced in a noise-free environment, to isolate and describe the GPR features of the potential targets in clear and well known conditions. This choice allows for a better description and classification of the GPR outputs. Moreover, the underground quarry environment is, in the overall, a quite noise free environment from the electromagnetic point of view. Performing the same synthetic simulations with the addition of a white noise to the synthetic data would be not particularly realistic. Eventual noise sources that could affect the real data are related to geological variability behind the excavation front and these are not easy to be simulated. Notwithstanding this eventual variability, under most of the simulated conditions, the correspondence of synthetic and real radargrams can be easily established, allowing for a combined evaluation of the GPR potentiality in the quarry environment.

3.2 Field data acquisition and processing

Radar data were acquired on the excavation faces with a K2 IDS Georadar system and 70 MHz, 200 MHz and 500 MHz frequency antennas. After preliminary data analysis, the 200 MHz antenna was selected as the more adequate, providing the better combination of investigation depth (3-4 m) and vertical resolution (0.1-0.2 m). The time-depth conversion on the axis perpendicular to the excavation faces was performed using a constant value of propagation velocity, evaluated from the modelling of subsurface scattering diffractions (fitting hyperbolae). The velocity values obtained by hyperbola fitting of acquired GPR data was 0.09 m/ns that is consistent with the theoretical value of electrical permittivity reported in Table 1.

Experimental data were acquired on the excavation faces with parallel profiles in horizontal and vertical directions, aiming to cover the entire surface of the faces. A similar scheme was used for all the acquisitions, with 6-8 horizontal and 3 vertical profiles, depending on logistical issues. Figure 3b shows an example acquisition scheme, with the resulting data oriented with respect to the excavation drill. For the acquisitions, appropriate elevation machinery (see Figures 9a and 12a) have been used to reach the top of the excavation face and move laterally within it.

Acquired data were processed with Reflexw5.0 (Windows OS) software using the most suitable processing flow to maximise the signal/noise ratio and to emphasize the information content. The processing flow for all the radargrams reported in the following was composed of: two static corrections (move start-time: to eliminate the first 10 ns, correspondent to the passing of the radar pulse in the air before reaching the rock, and time cut: to limit the investigated range to 100 ns), a dewowing filter with time window of 10 ns, two gain operations (a compensation for geometrical divergence with scaling factor of 0.4 and a gain function, defined as $g(t) = (1 + \frac{0.2}{pulse\ width} t)e^{(\frac{0.02}{8.69}t)}$) and a removal of the background noise (based on the average of all the traces).

In order to visualize the spatial distribution of the anomalies behind the excavation faces, the single radar profiles were combined to build a three-dimensional volume with Voxler software. Horizontal and vertical radargrams were juxtaposed as shown in Figure 3b and elaborated to create a 3D reconstruction of the anomalies. For this aim, an appropriate colour scale representing absolute radar amplitudes (Figure 3b) was adopted for all the presented Figures. Anomalies were identified based on appropriate thresholds on this colour scale. The value of imposed thresholds varies depending on the permittivity contrast between the gypsum and the anomaly and on the depth of the anomaly itself.

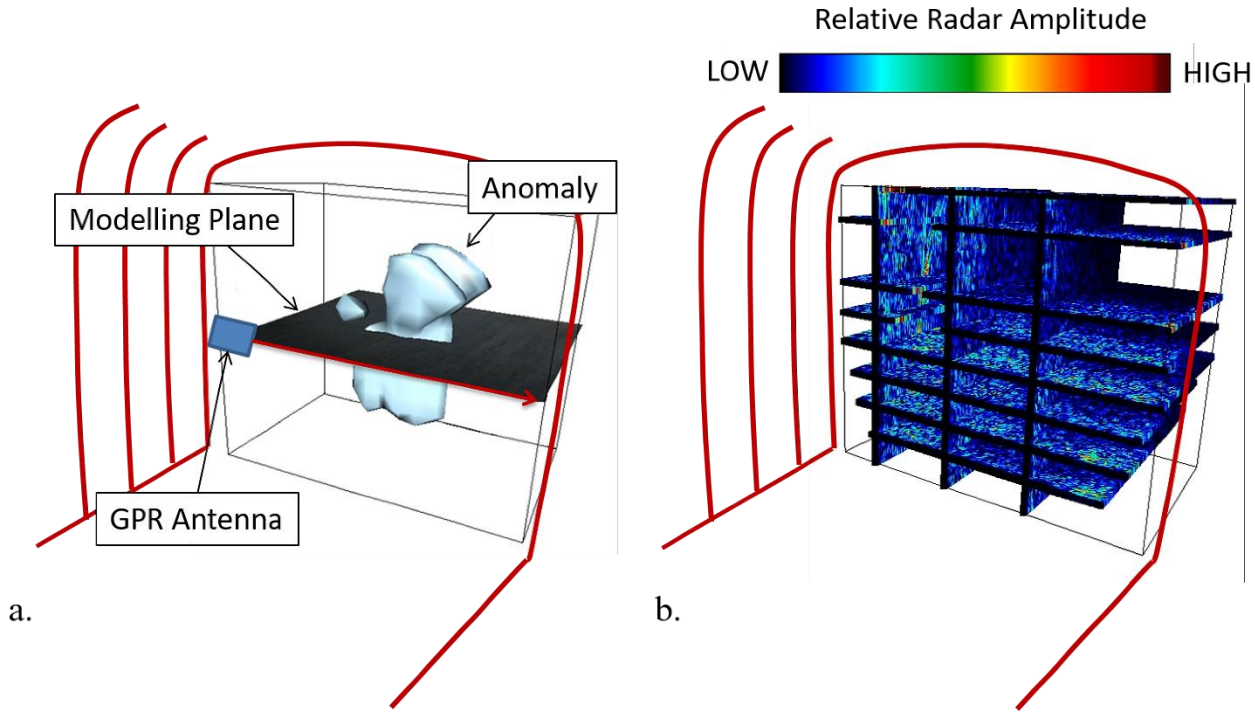

Figure 3 a. Geometrical orientation of the numerical models with respect to the quarry face and a generic simulated anomaly. b. General radar acquisition scheme on the quarry faces.

4 Modeling results

4.1 Conduits

The presence in the orebody of karst conduits was simulated with a circular anomaly with diameter of 20 cm in a homogeneous volume of gypsum (Fig. 4a). Synthetic radargrams in case of empty conduit (Fig. 4b) and water-filled conduit (Fig. 4c) were simulated. Results show, in both the

simulations, a hyperbolic signal with apex coincident with the position of the circular anomaly. In the case of water-filled conduit, multiple hyperbolae are recognizable under the principal one. The presence of water indeed triggers a ringing phenomenon and multiple hyperbola are created when the radar-wave passes through the fluid (Fig. 4c). On the contrary, when the conduit is empty, the high radar-wave propagation velocity in air brings to an overlap of the multiple hyperbola (fig. 4b). Different models with increasing depth of the anomaly where also produced, confirming the anomaly visibility till a maximum investigation depth of 5 m.

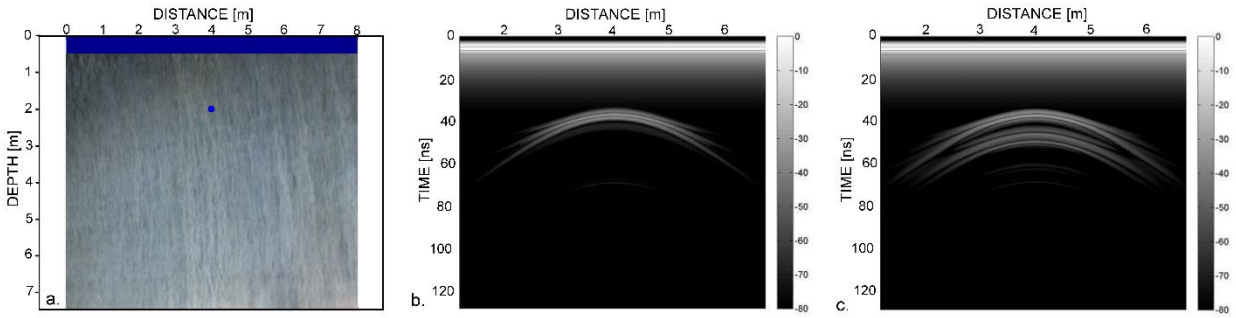

Figure 4 a. Reference model with a cylindrical anomaly with diameter of 20 cm at a depth of 1.5 m in an uniform volume of gypsum; b. Synthetic radargram with the anomaly considered as void; c. Synthetic radargram with the anomaly considered as filled of water.

4.2 Cavities

Figure 5a shows a model simulating the presence of a karst cavity with regular shape and size of 1m x 1m. Results refer to the absence of filling and to the presence of water within the anomaly (respectively, Figure 5b and 5c). In both simulated radargrams, the interference of several hyperbolic signals producing a big and complex anomaly is evidenced. The absence of filling brings to a further multiplication of signal reflections (ringing) within the void cavity (Fig. 5b). These reflections are strongly attenuated in the water-filled cavity (Fig. 5c), where the signal is less complex and more defined. In this last condition, main reflections of the top and the bottom of the cavity are possible to be recognized. The presence of water seems therefore to generate opposite effects in the simulations of small conduits and big cavities. In the first case, an increased ringing due to the anomaly is recognized (Fig. 4c), while in the second case the ringing is strongly reduced (Fig. 5c). This apparent

inconsistency can be explained considering the size of the anomalies compared to the radar velocity in water or air: in small dimensions anomalies (conduits) the velocity reduction due to water makes the arrival times of multiple reflections at the anomaly borders shortly delayed and partially superimposed in the acquisition time; in anomalies with greater dimensions (cavities) the arrival times are instead strongly delayed and do not superimpose in the acquisition time. The opposite is true for the air filled anomalies. These considerations are related to the fact that the arrival times of different reflection events is related both to the space travelled (anomaly dimensions) and to the velocity of propagation within this space (filling material).

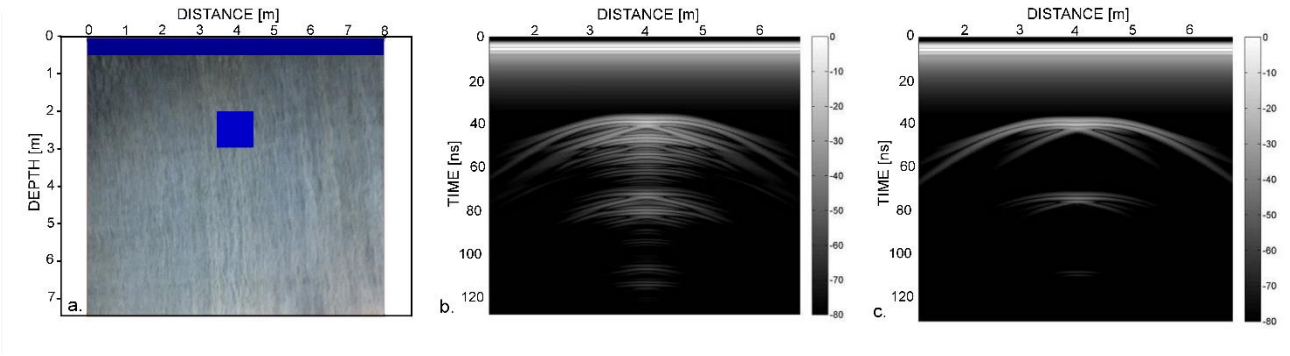

Figure 5 a. Reference model with a square anomaly with sizes of 1mx1m at a depth of 1.5 m in an uniform volume of gypsum; b. Synthetic radargram with the anomaly considered as void; c. Synthetic radargram with the anomaly considered as filled of water.

The framework of a natural rock mass may present complex situations where the schematization of a square cavity with regular shape is insufficient to correctly interpret the GPR outputs. Differences in position, sizes and shape of the cavity can significantly influence the GPR results. With this aim different cavity shapes and position were further simulated (also in comparison with the following acquired experimental data). Figure 6 shows an example of a different cavity shape and location. The cavity modelled in Figure 6a, located at the left of the investigated face, with a sharp tip towards the centre of the section, gives an output considerably different from the idealized square cavity in Figure

5. Still this water filled cavity is clearly recognized and approximate cavity dimensions can be deduced from the radargram considering top and bottom reflections.

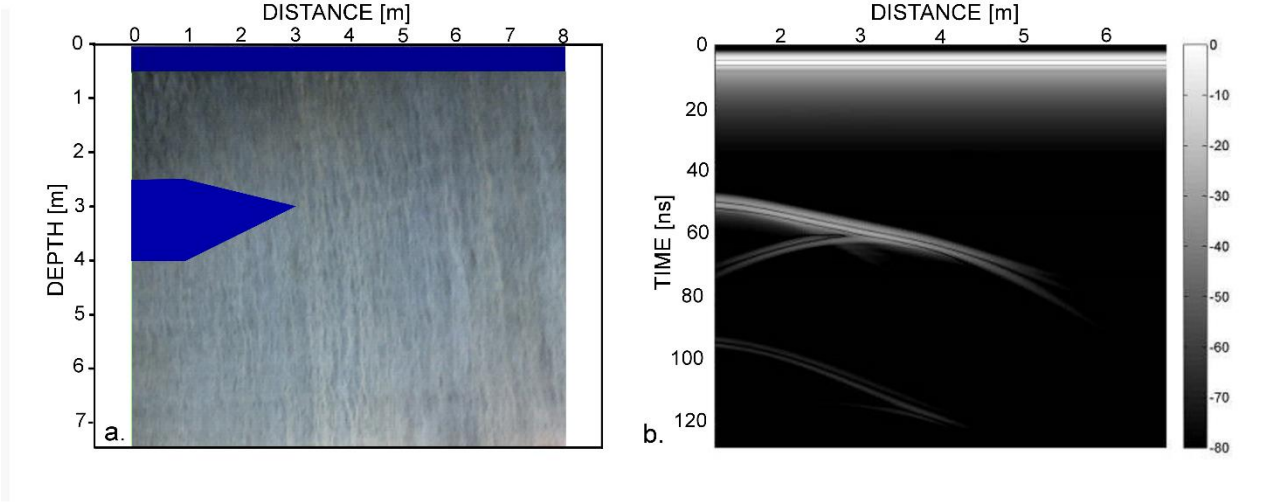

Figure 6 a. Reference model with carst cave with irregular shape at a depth of 2 m in an uniform volume of gypsum; b. Synthetic radargram with the anomaly considered as filled by water.

Another potential complex situation is due to the interference of a cavity with lateral conduits, possibly responsible of the alimentation and the connection with the karst system. Fig. 7a presents a schematic model of this situation.

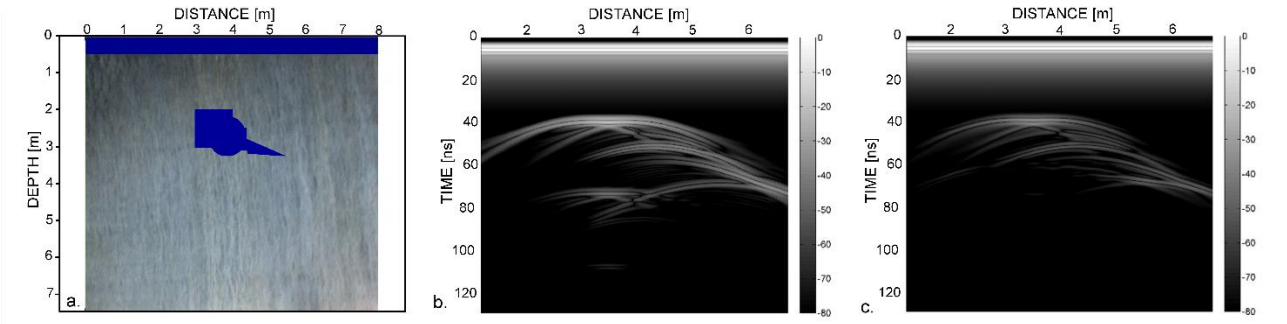

Figure 7 a. Reference model with carst cave connected with a conduit at a depth of 1.5 m in an uniform volume of gypsum; b. Synthetic radargram with the anomaly considered as filled of water; c. Synthetic radargram with the anomaly considered as filled of clay

The cavity with its conduit were considered as filled by water (Fig. 7b) or filled by clay (Fig. 7c) in the simulations. Results show a large hyperbolic signal, similar to Figure 5b, for the main cavity but

interfering with several closer hyperbolic signals in the right, where the conduit is located. The presence of clay within the cavity with respect to the water further slows down the radar velocity and increases the attenuation so that the reflection from the cavity bottom is no more visible in the simulated radargrams.

4.3 Fractures

The presence of a shallow open water-bearing fracture oriented almost perpendicular to the excavation face was simulated as shown in Figure 8a. Simulated fracture aperture was of about the same order of small conduits (i.e. 20 cm). The synthetic radargram shows one principal hyperbole intensified and complicated by the overlap with several hyperbolic signals in the right, where the fracture is oriented.

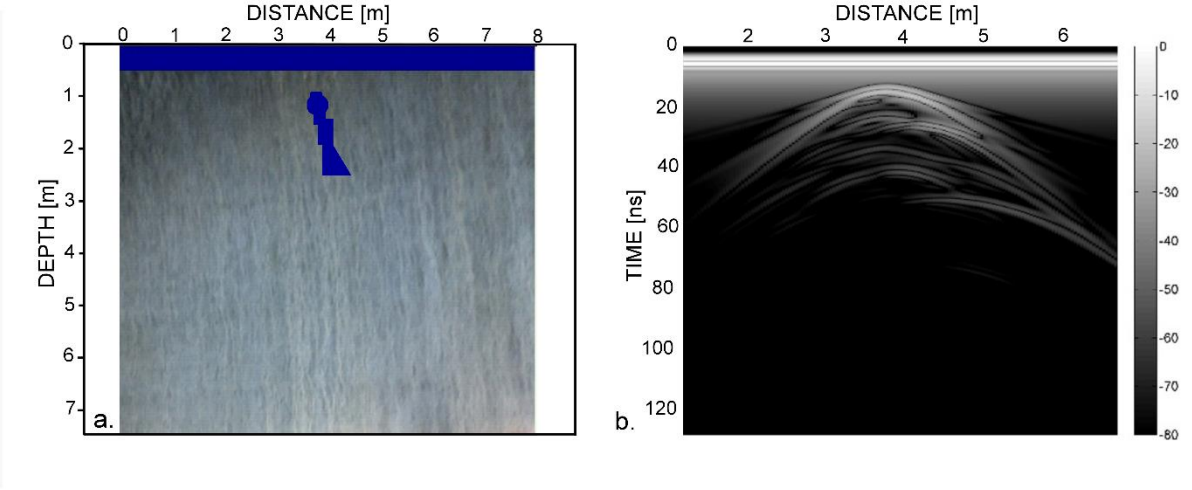

Figure 8 a. Reference model to simulate the presence of an open fracture almost perpendiculr to the excavation surface; b Simulated synthetic radargram with the anomaly considered as filled of water

5 Survey results

5.1 Conduits

An air filled drilled hole (10 cm diameter) was used to simulate a small karst conduit. As shown in Figure 9a, c and d, the hole is oriented almost perpendicular to the lateral wall of the drift, entering

the gypsum ore body on the side of the excavated gallery. Six vertical radar profiles at increasing distances from the hole were acquired along the "waved" wall, on the "wave-face" parallel to the drilled hole direction. The radar input is therefore directed toward the hole but the hole itself will result at increasing distances (from 1 to 6 "waves") from the antenna. Radar output for the shallower distance profile (Fig. 9b) gives a well-defined hyperbole, without multiple reflections, concordant with the model for a void conduit in Figure 4b.

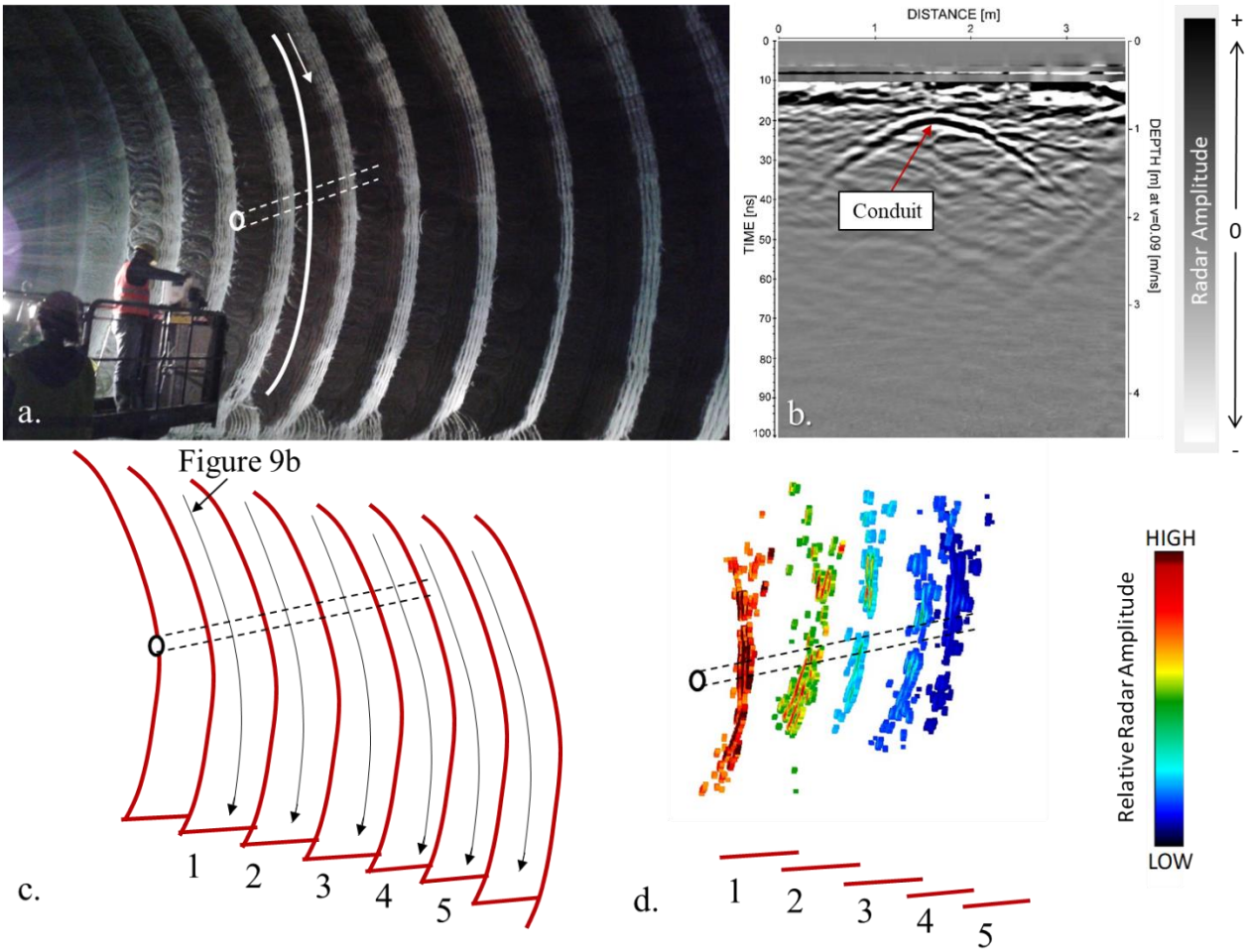

Figure 9 a. Radar acquisition of a drilled hole; b. Radar output with hole depth of 0.5 m; c. Acquisition scheme of the six profiles; d. Three-dimensional reconstruction

With the increasing distance from the hole, the signal results more attenuated, being completely obliterated from environmental noise in the sixth profile (distance from the hole of 2.5 m). This suggests a threshold for the investigation depth of the method (Caselle et al. 2016). This threshold is

significantly lower than the one evidenced with numerical simulations, given the added background noise. The hyperbola apexes from the different profiles are aligned and their depth coherently increases. Since the processing flow was uniform for all the profiles, the hyperbolic signal has decreasing amplitude with the increase of the depth. Therefore, in the three-dimensional reconstruction in Figure 9d, decreasing values of threshold amplitude were imposed to the GPR profiles with increasing distance from the target. Still, results from this visualization allow for a correct evaluation of the elongation direction and spatial position of the hole. These results suggest that the identification of small karst conduits with different parallel profiles is possible.

5.2 Cavities

A GPR profile was acquired on the excavation face in front of the karst room cropped out after the 2005 inrush in Moncalvo quarry (Fig. 10a). The radar output (Fig. 10b) shows, in the right, a marked, multiple ringing signal referable to the cavity. The absence of filling bring to create, as in the model in Figure 5b, a complex output due to the multiple reflections (ringing) of the signal within the void cavity.

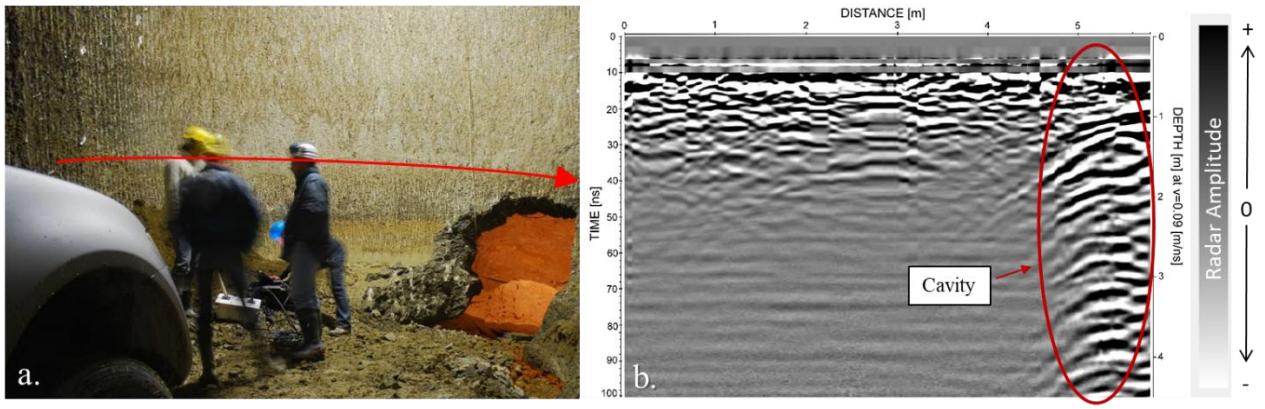

Figure 10 a. Excavation face in front of the karst room cropped out after the 2005 inrush; b. Radar output

Two quarry faces were also selected (one from Moncalvo quarry and one from Calliano quarry) to test the detectability of cavities filled by water. In the tested faces, the excavations have been interrupted because the drilling of horizontal boreholes highlighted the presence of water, that, as

shown in Figures 11a and 12a, was actually stilling from the holes when the present study was performed. Surveys were therefore devoted to the potential identification of the water cavities or karst conduits alimenting these stillings.

Figure 11 refers to the GPR data acquired in the Moncalvo quarry. Fresh pressurized water flows through the vent in the high-left portion of the excavation face (Fig.11a). Radar acquisition was performed following the scheme in Figure 11c. An example horizontal GPR profile shows, in the left, a complex signal due to the interference of two hyperbolae at different depths and x-position (Fig. 11b). The radar anomaly is significantly similar to the one simulated in Figure 6, suggesting a geometrically similar situation. Three-dimensional reconstruction (Fig. 11d) shows the good alignment of the hyperbolic signals from horizontal and vertical profiles, with concordant position and depth. From these multiple profiles alignments, the estimation of the approximate location and dimensions of the water filled void is therefore possible.

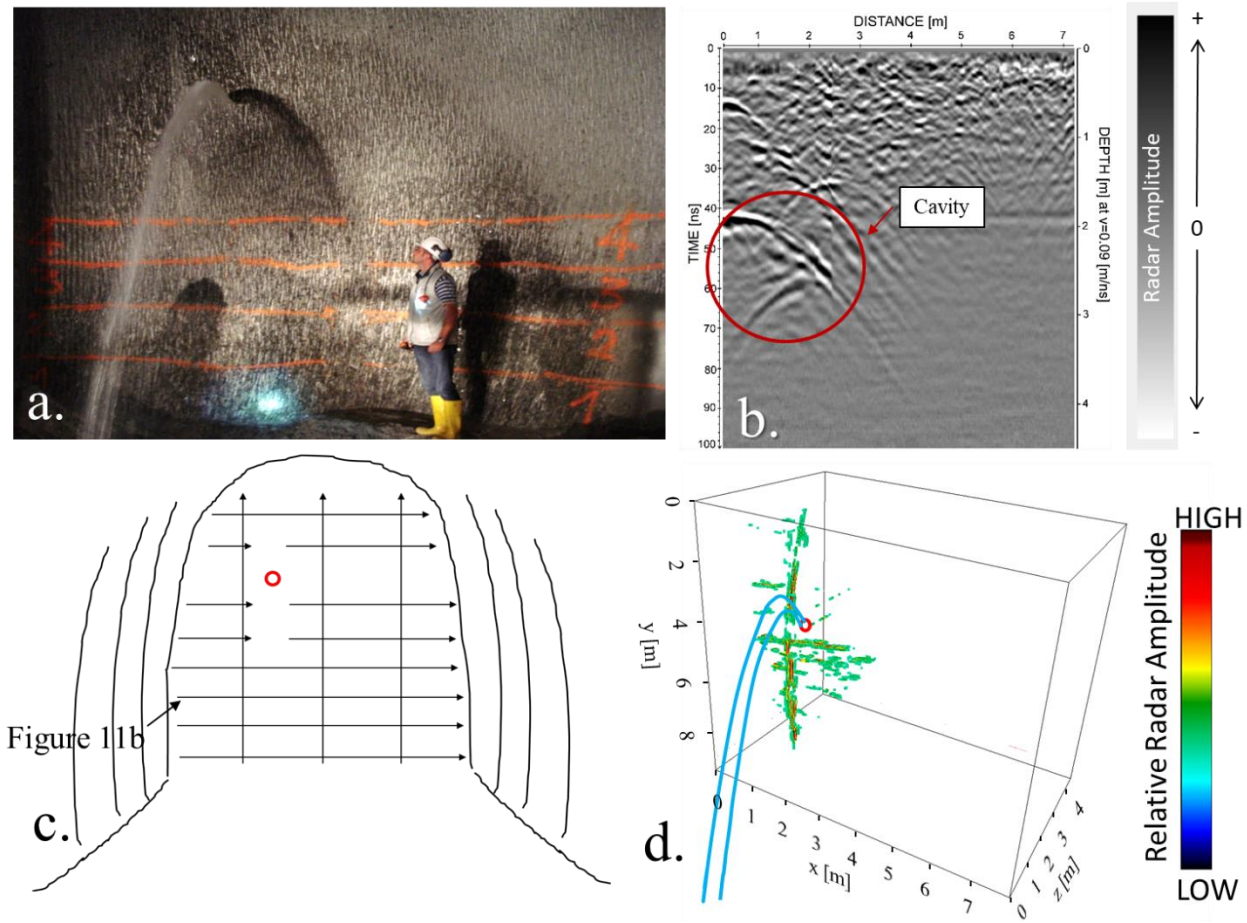

Figure 11 a. Excavation front in Moncalvo quarry with water leakage.; b. Radar output from an horizontal profile; c. Acquisition scheme used for radar profiles; d. Three-dimensional reconstruction.

Figure 12 refers to the water leakage in the underground Calliano quarry. When this study was performed, water was flowing through three holes in the lower part of the excavation face. GPR profiles were acquired following the acquisition scheme in Fig. 12c. Output of the second horizontal profile from the bottom shows a well-defined anomaly due to the interference of 3 hyperbolae with apexes at 1, 2.5 and 3.5 m from the profile start (Fig. 12b). A strong signal at 75ns (about 3.5 m) can be attributed to the end of the investigated wall (which has a thickness of about 3-4 m). Similar evidences may be recognized in all the horizontal profiles. Vertical profiles show continuous horizontal reflectors for their entire height. Figure 12d shows the 3d volume reconstruction. Signals from vertical and horizontal profiles delineate a large area in the bottom of the excavation front potentially interested by the water-filled cavity.

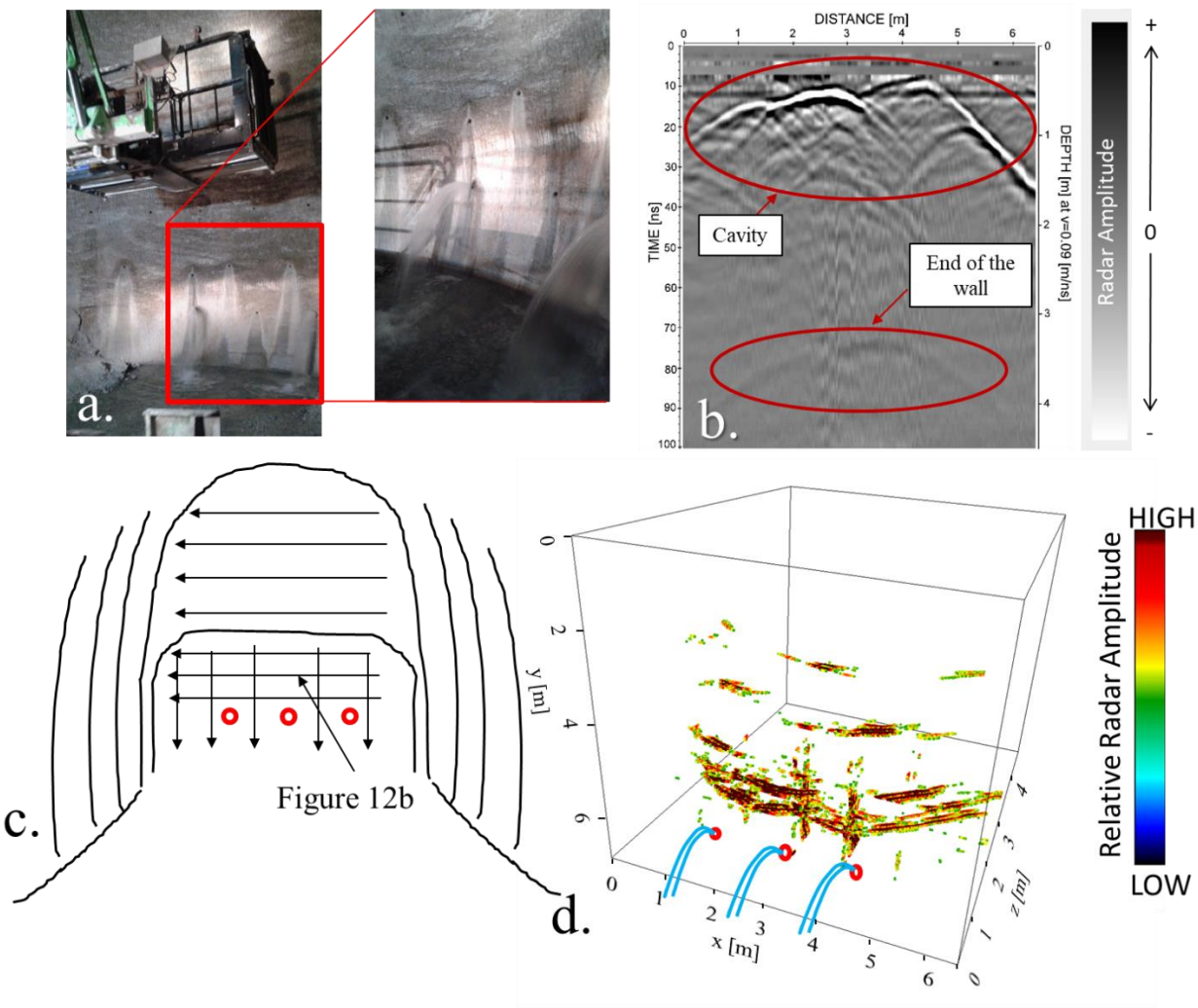

Figure 12 a. Excavation front with water leakage in Calliano quarry; b. Radar output from an horizontal profile; c. Acquisition scheme used for radar profiles; d. Three-dimensional reconstruction.

Figure 13 describes the radar investigation of a potential clay-filled cavity in the Calliano quarry. A compact clay body was observed through an opening in the low-left part of the drift face (Fig. 13a). Radar analyses were performed following the investigation scheme in Figure 13c. GPR outputs show the presence of well-defined hyperbolic anomalies in the horizontal profiles (e.g. the lower complete horizontal profile in Fig. 13b). The vertical profile above the opening contains a clear reflector dipping towards the opening in the low part of the wall. The resulting 3d reconstruction (Fig. 13d), synthetizing the information from horizontal and vertical profiles, shows the good agreement of the signals in the single profiles, concordant to describe the presence of an inclined anomalous body.

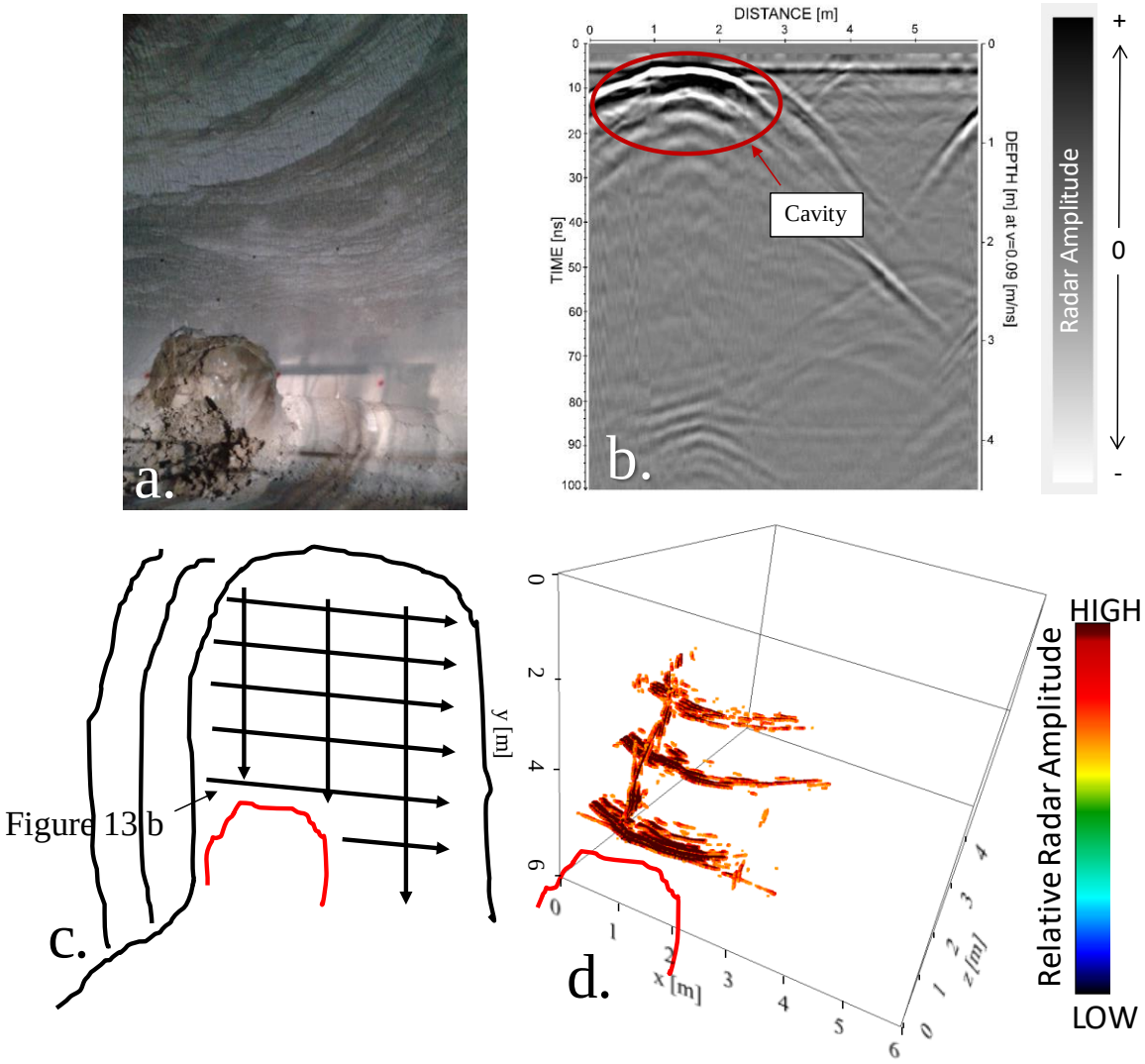

Figure 13 a. Excavation face with outcropping of a clay body; b. Radar output from an horizontal profile; c. Acquisition scheme used for radar profiles; d. Three-dimensional reconstruction

5.3 Fractures

An open sub-vertical fracture was recognized and analysed in the Calliano quarry (Figure 14a). The analysis with GPR, performed with vertical and horizontal profiles following the scheme in Figure 14c, shows an acceptable detectability of the structure. Horizontal profiles (e.g. Fig. 14b) report local hyperbolic anomalies, moving to the left on the top of the face, reproducing the orientation of the fracture. An intensification of the signal in the right branch of the hyperbole suggests an orientation of the structure in that direction, in agreement with the synthetic radargram in Figure 8b.

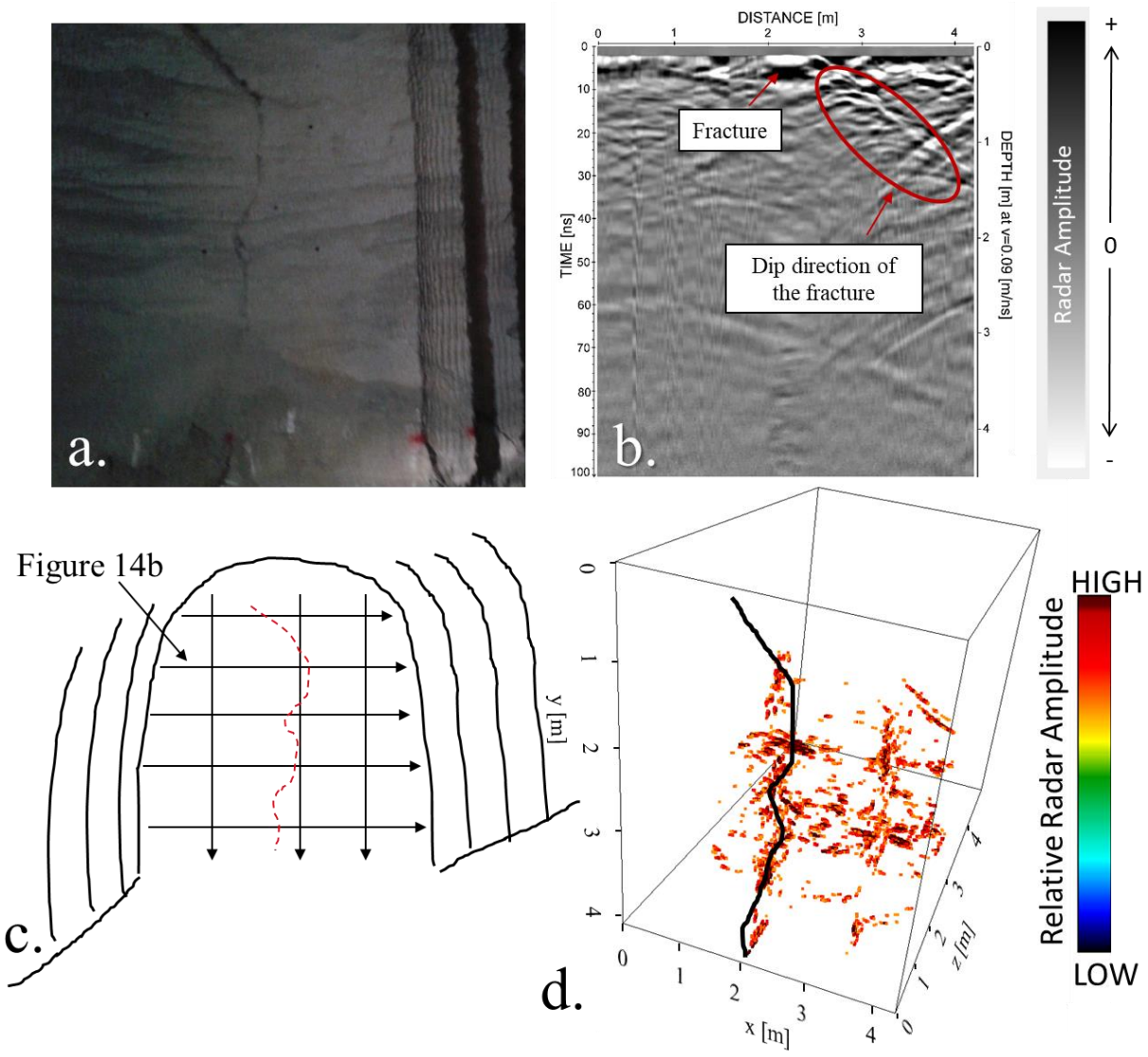

Figure 14 a. Excavation front with the open sub-vertical fracture; b. Radar output from an horizontal profile; c. Acquisition scheme used for radar profiles; d. Three-dimensional reconstruction.

With respect to numerical simulations, reduced ringing effect was evidenced in the acquired data, suggesting the presence of an open fracture with air filling. This is corroborated by the absence of water inflows at the excavation face. The additional reflection in the right part of the radargram at about 80 ns (Fig. 14b) is probably due to the radar reflection on the lateral wall of the analysed face. Vertical profiles, subparallel to the fracture outcrop, contain vertical signals, oriented parallel to the face. The 3d reconstruction (Figure 14d) shows concentrations of anomalies in correspondence of the fracture cropping and in the right part of the volume. This last part can be related to the reflection of

the signal on the lateral wall for increased times, but also to a potential parallel fracture with the one evidenced in the front.

6 Discussions and Conclusions

The principal elements of karst hazard (conduits, cavities and fractures) in gypsum orebodies were investigated and analyzed with Ground Penetrating Radar (GPR) techniques. Electromagnetic models were produced for each anomaly, considering the influence of different possible fillings (air, water and clay). The geological complexity was considered in the modeling of karst caves to obtain more realistic frameworks. Models show clear outputs for all the considered situations. The discrimination between empty and water-filled anomalies was possible thanks to the different propagation velocities and absorption power. Particularly, small karst conduits, or fractures, filled with water are evidenced by the presence of localized hyperbolic signals and increased ringing effects with respect to the same anomalies filled with air. Cavities are instead evidenced by more complicated reflection patterns, related to their shapes and dimensions; the ringing effect is promoted in presence of air with respect to water or clay fillings.

A wide GPR survey campaign was performed in two underground gypsum quarries with evidences of karst phenomenon. Targets ahead the excavation faces were investigated through horizontal and vertical GPR profiles. Output radargrams were processed and described. Three-dimensional reconstructions were proposed, aiming to create an easily understandable and complete visualisation of the GPR outputs.

From a comparison of both numerical simulations and field surveys, it was possible to evaluate the potentiality of GPR for the present case study, in particular:

- Karst conduits: a successful identification of karst conduits with diameter above 10 cm was verified up to a depth of about 2 m. The radar output is a single hyperbolic signal with apex coincident with the position of the circular anomaly. Potential discrimination with respect to

the water filling of these conduits are also evidenced. These last discriminations are related to the presence or not of multiple hyperbolic reflections for the same spatial location. In case of water within the conduits, the ringing phenomenon due to the slowing of the radar signal is indeed promoted (see Figures 4c and 7b) with respect to the presence of air within the conduit (see Figures 4b and 9b);

- Karst cavities: a successful identification of karst cavities has been obtained in all the simulated and real acquisitions. The radar output consists of a large and very intense anomaly, resulting by the interference of several hyperbolic signals. Cavities with irregular shapes may complicate the radar anomalies, creating big and complex signals. Contrary to the results obtained over karst conduits, air filled cavities are depicted with increasing ringing phenomenon (see Figures 5b and 10b) with respect to clay or water filled cavities (see Figures 5c, 11b and 12b). This last effect can be related to the increased attenuation of the radar signal in presence of clay or water which does not allow multiple reflections within the same cavity. In the case of water or clay filling, the bottom of the cavity is also not always possible to be discriminated, depending on the depth of the cavity (see Figures 7b and 7c).
- Open fractures: if the fracture is oriented perpendicular (or almost perpendicular) to the excavation face, the radar output can be described as a principal hyperbole intensified and complicated by the overlap with several hyperbolic signals in the direction where the fracture is oriented. Having similar dimensions to karst conduits, also in open fractures the water filling promotes the radar wave ringing with respect to the air filling (see Fig. 8b with respect to Fig. 14b). Open fractures perpendicular to the excavation face are critical to be identified in terms of dipping direction.

For exploitation purposes, the assessment of the dangerousness of a structure and the assignment of a specific warming degree to each GPR scenario is fundamental. Taking as reference the radar output relative to an undisturbed quarry face (Figure 15), all the presented anomalies are detectable and a first degree of warming could be assigned to all those situations. Additional discriminations can be based on the size of the anomaly and, particularly, on its filling. Results of this study indicate a good

detectability of the size of the anomaly on the base of the lateral extension of the hyperbolic signal (or the combined signal of several hyperbolae). The assessment of the approximate size of the anomaly is not only important in itself for the warming purposes, but also for the discrimination of the filling. Indeed, as already claimed, the water filling has different effects on the GPR output depending on the size of the anomaly. The presented study offers therefore a preliminary guide to predict the dangerousness of a quarry face on the base of GPR analyses.

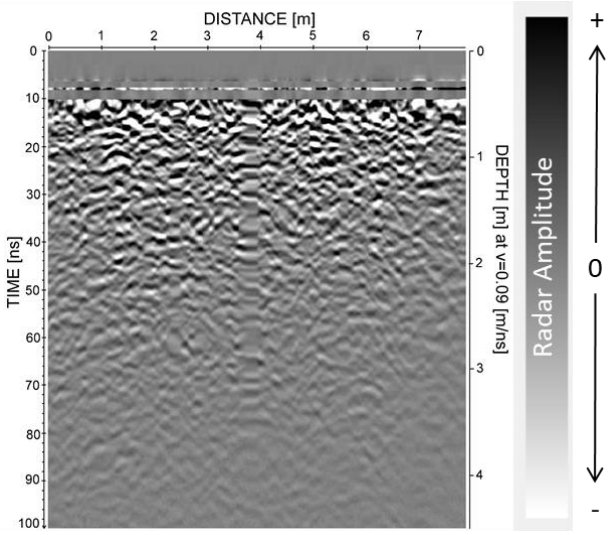

Figure 15 Radar output in correspondence of an undisturbed, integer quarry face, without the presence of anomalies.

For the low investigation depth of GPR survey method (about 3 meters within this material), a suitable way to apply this technique would include the implementation of a system of continuous automatic monitoring. A continuous upgrade of GPR imaging of the gypsum orebody, concomitant with the excavation progress, would provide reliable previsions, with positive effects on the safety and the efficiency of the exploitation. With this aim the data migration was not included in the processing flow in order to maintain a fast and light data processing, in view of a possible real-time application of the methodology, concomitant with the excavation progress.

Two examples of application of migration process on the experimental data are shown hereafter in Figures 16 and 17. As could be expected, the migration significantly affects the data visualization

when a single clear hyperbolic pattern is recognized (conduits example in Figure 16). In this case, the hyperbole collapses in a single point better visualizing the drilled hole shape and dimensions. However, the migration process only improves the imaging quality but the delectability of the conduit is not particularly increased. On the contrary, the presence of a point instead of a hyperbole is more difficult to be recognized at higher depths.

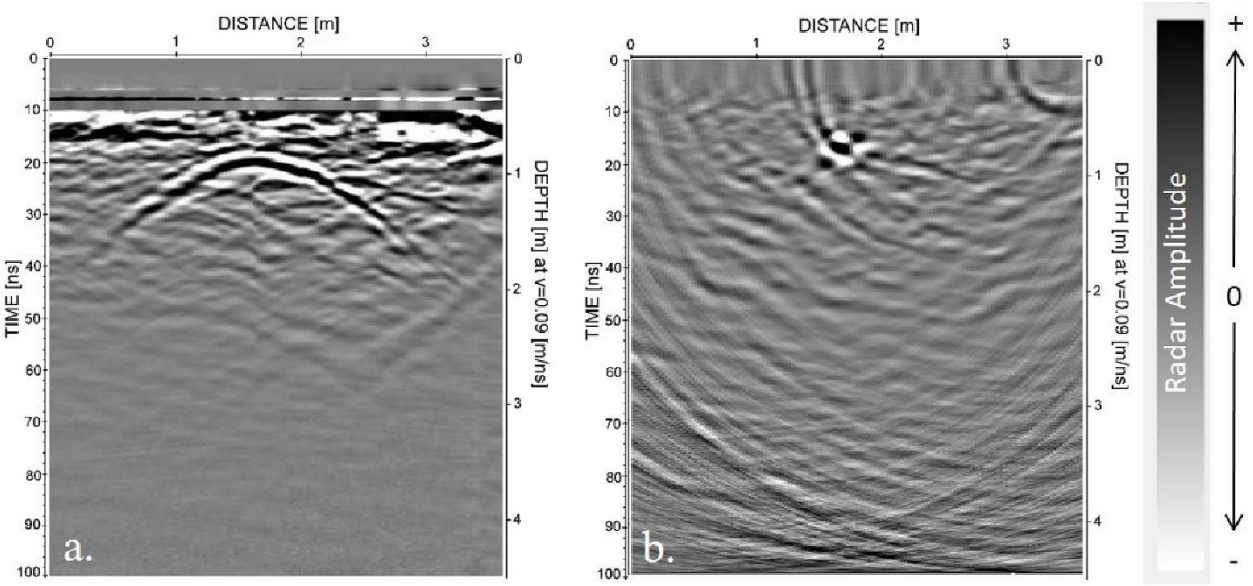

Figure 16 Migration process of data referred to a karst conduit (figure 9b).

Similar considerations can apply in the presence of a karst cavity (Figure 17). The migrated image better allows to define the real cavity shape by collapsing multiple reflection patterns on its boundaries.

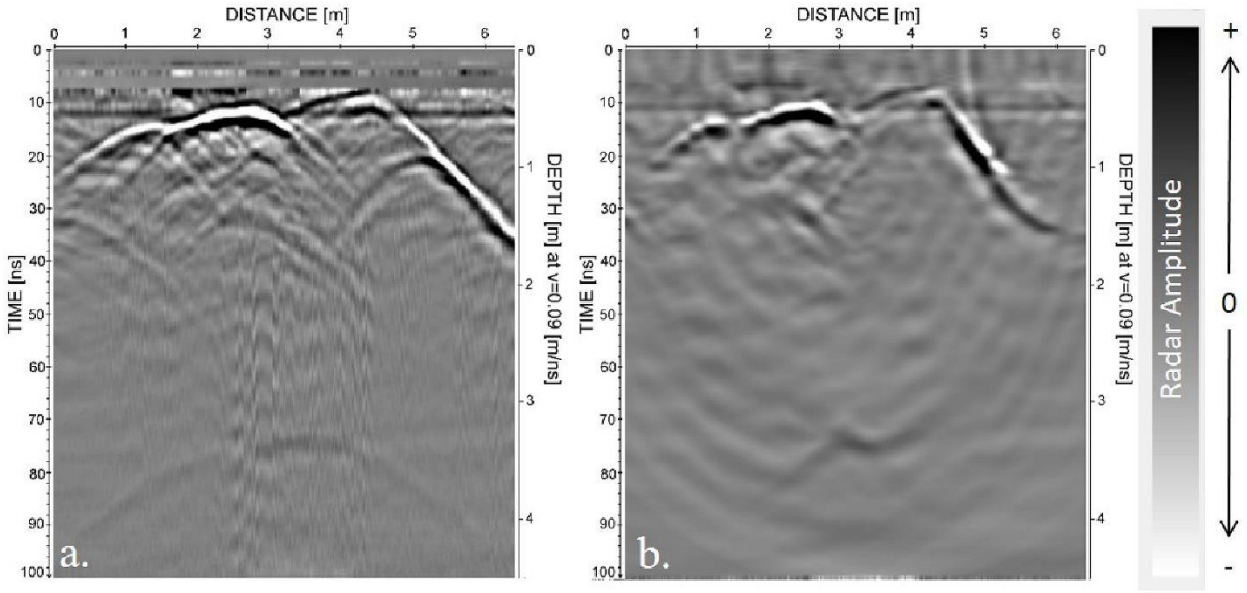

Figure 17 Migration process on data referred to a karst cavity (figure 12b).

Nevertheless, again, if the survey results have to be used for preliminary warning purposes, even under the eyes of non GPR expert users, the non migrated radargrams contain more signal and information that can allow for the recognition of an anomaly in the gypsum formation. Based on this, a clear warning can be established. After this warning, shape and filling discriminations could be performed by more sophisticated processing (including migration) and by comparison with synthetic simulations reported in this paper.

Acknowledgements

The Authors are indebted with the anonymous private company that indicated the location of suspected anomalies within the quarry, allowed the execution of the field surveys and financed the research.

References

Afshar, A., Abedi, M., Norouzi, G.-H., Riahi, M.-A., 2015. Geophysical investigation of underground water content zones using electrical resistivity tomography and ground penetrating radar: A case study in Hesarak-Karaj, Iran. Eng. Geol. 196, 183–193. https://doi.org/10.1016/j.enggeo.2015.07.022

Aldas, G.U., Kadioglu, S., Ulugergerli, E., 2006. The usage of ground penetrating radar (GPR) in designing blast pattern. Rock Mech. Rock Eng. 39, 281–290. https://doi.org/10.1007/s00603-005-0074-3

Bonetto, S., Fiorucci, A., Fornaro, M., Vigna, B., 2008. Subsidence hazards connected to quarrying activities in a karst area: the case of the Moncalvo sinkhole event (Piedmont, NW Italy). Est. J. Earth Sci. 57, 125. https://doi.org/10.3176/earth.2008.3.01

Bonetto, S., Fornaro, M., 2005. Subsidence events related to natural conditions and gypsum quarrying activity in the Monferrato area (Piedmont, NW Italy). Presented at the In Proceedings of MAEGS14 - 14th Meeting of the Association of European Geological Societies, Torino, 19-23 September 2005, pp. 61-62, -, p. .

Bowling, J.C., Rodriguez, A.B., Harry, D.L., Zheng, C., 2005. Delineating alluvial aquifer heterogeneity using resistivity and GPR data. Ground Water 43, 890–903. https://doi.org/10.1111/j.1745-6584.2005.00103.x

Caselle, C., Bonetto, S., Comina, C., Stocco, S., 2016. Preliminary evaluation of In-mining GPR surveys for the identification of karst anomalies in a gypsum quarry. 1st Conference on Geophysics for Mineral Exploration and Mining, Near Surface Geoscience

Caselle, C., Penone, A., Bonetto, S., 2018. Preliminary mechanical characterisation of gypsum rock using UCS and Point Load Test correlation. Geoingegneria Ambientale e Mineraria 153, 60–67.

Caselle, C., Bonetto, S., Colombero, C., Comina, C., 2019a. Mechanical properties of microcrystalline branching selenite gypsum samples and influence of constituting factors. Journal of Rock Mechanics and Geotechnical Engineering 11(2), 228-241. https://doi.org/10.1016/j.jrmge.2018.09.003

Caselle, C., Umili, G., Bonetto, S., Ferrero, A.M., 2019b. Application of DIC analysis method to the study of failure initiation in gypsum rocks. Géotechnique Letters 9(1), 35-45. https://doi.org/10.1680/jgele.18.00156

Caselle, C., Bonetto, S., Vagnon, F., Costanzo, D., 2019c. Dependence of macro mechanical behaviour of gypsum on micro-scale grain-size distribution. Géotechnique Letters, *In Press*. https://doi.org/10.1680/jgele.18.00206

Clari, P., Pierre, F.D., Novaretti, A., Timpanelli, M., 1995. Late Oligocene-Miocene sedimentary evolution of the critical Alps/Apennines junction: the Monferrato area. Northwestern Italy. Terra Nova 7, 144–152. https://doi.org/10.1111/j.1365-3121.1995.tb00683.x

Daniels, D.J., 2004. Ground Penetrating Radar. IET.

Dela Pierre, F., Bernardi, E., Cavagna, S., Clari, P., Gennari, R., Irace, A., Lozar, F., Lugli, S., Manzi, V., Natalicchio, M., Roveri, M., Violanti, D., 2011. The record of the Messinian salinity crisis in the Tertiary Piedmont Basin (NW Italy): The Alba section revisited. Palaeogeogr. Palaeoclimatol. Palaeoecol. 310, 238–255. https://doi.org/10.1016/j.palaeo.2011.07.017

Dérobert, X., Abraham, O., 2000. GPR and seismic imaging in a gypsum quarry. J. Appl. Geophys. 45, 157–169. https://doi.org/10.1016/S0926-9851(00)00025-2

Gómez-Ortiz, D., Martín-Crespo, T., 2012. Assessing the risk of subsidence of a sinkhole collapse using ground penetrating radar and electrical resistivity tomography. Eng. Geol. 149–150, 1–12. https://doi.org/10.1016/j.enggeo.2012.07.022

Jiang, H.-M., Li, L., Rong, X.-L., Wang, M.-Y., Xia, Y.-P., Zhang, Z.-C., 2017. Model test to investigate waterproof-resistant slab minimum safety thickness for water inrush geohazards. Tunn. Undergr. Space Technol. 62, 35–42. https://doi.org/10.1016/j.tust.2016.11.004

Kovin, O., 2011. Mapping of evaporite deformation in a potash mine using ground penetrating radar: Upper Kama deposit, Russia. J. Appl. Geophys. 74, 131–141. https://doi.org/10.1016/j.jappgeo.2011.04.009

Li, S., Liu, B., Xu, X., Nie, L., Liu, Z., Song, J., Sun, H., Chen, L., Fan, K., 2017. An overview of ahead geological prospecting in tunneling. Tunn. Undergr. Space Technol. 63, 69–94. https://doi.org/10.1016/j.tust.2016.12.011

Mahmoudzadeh, M.R., Francés, A.P., Lubczynski, M., Lambot, S., 2012. Using ground penetrating radar to investigate the water table depth in weathered granites - Sardon case study, Spain. J. Appl. Geophys. 79, 17–26. https://doi.org/10.1016/j.jappgeo.2011.12.009

Orlando, L., 2003. Semiquantitative evaluation of massive rock quality using ground penetrating radar. J. Appl. Geophys. 52, 1–9. https://doi.org/10.1016/S0926-9851(02)00229-X

Piana, F., Polino, R., 1995. Tertiary structural relationships between Alps and Apennines: the critical Torino Hill and Monferrato area. Northwestern Italy. Terra Nova 7, 138–143. https://doi.org/10.1111/j.1365-3121.1995.tb00682.x

Porsani, J.L., Sauck, W.A., Júnior, A.O.S., 2006. GPR for mapping fractures and as a guide for the extraction of ornamental granite from a quarry: A case study from southern Brazil. J. Appl. Geophys. 58, 177–187. https://doi.org/10.1016/j.jappgeo.2005.05.010

Pueyo Anchuela, Ó., López Julián, P., Casas Sainz, A.M., Liesa, C.L., Pocoví Juan, A., Ramajo Cordero, J., Pérez Benedicto, J.A., 2015. Three dimensional characterization of complex mantled karst structures. Decision making and engineering solutions applied to a road overlying evaporite rocks in the Ebro Basin (Spain). Eng. Geol. 193, 158–172. https://doi.org/10.1016/j.enggeo.2015.04.022

Pueyo-Anchuela, Ó., Soriano, A.P.J., M.A., Casas-Sainz, A.M., 2009. Characterization of karst hazards from the perspective of the doline triangle using GPR - Examples from Central Ebro Basin (Spain). Eng. Geol. 108, 225–236. https://doi.org/10.1016/j.enggeo.2009.06.022

Sevil, J., Gutiérrez, F., Zarroca, M., Desir, G., Carbonel, D., Guerrero, J., Linares, R., Roqué, C., Fabregat, I., 2017. Sinkhole investigation in an urban area by trenching in combination with GPR, ERT and high-precision leveling. Mantled evaporite karst of Zaragoza city, NE Spain. Eng. Geol. 231, 9–20. https://doi.org/10.1016/j.enggeo.2017.10.009

Vigna, B., D'Angeli, I., Fiorucci, A., Waele, J.D., 2017. Hydrogeological flow in gypsum karst areas: some examples from northern Italy and main circulation models. Int. J. Speleol. 46. https://doi.org/ https://doi.org/10.5038/1827-806X.46.2.2095

Vigna, B., Fiorucci, A., Banzato, C., Forti, P., De Waele, J., 2010. Hypogene gypsum karst and sinkhole formation at Moncalvo (Asti, Italy). Z. Für Geomorphol. Suppl. Issues 54, 285–306. https://doi.org/10.1127/0372-8854/2010/0054S2-0015

Wai-Lok Lai, W., Dérobert, X., Annan, P., 2018. A review of Ground Penetrating Radar application in civil engineering: A 30-year journey from Locating and Testing to Imaging and Diagnosis. NDT E Int. 96, 58–78. https://doi.org/10.1016/j.ndteint.2017.04.002

Wu, J., Li, S.-C., Xu, Z.-H., Zhao, J., 2019. Determination of required rock thickness to resist water and mud inrush from karst caves under earthquake action. Tunn. Undergr. Space Technol. 85, 43–55. https://doi.org/10.1016/j.tust.2018.11.048

Xu, Z.H., Wu, J., Li, S.C., Zhang, B., Huang, X., 2018. Semianalytical solution to determine minimum safety thickness of rock resisting water inrush from filling-type karst caves. Int. J. Geomech. 18. https://doi.org/10.1061/(ASCE)GM.1943-5622.0001071